Models, Algorithms and Error Estimation for Computational Viscoelasticity ⋆

Marianna Karamanou [a], Simon Shaw [a], MK Warby [a] and JR Whiteman [a]

[a] *BICOM and Department of Mathematical Sciences, Brunel University, Uxbridge, England, UB8 3PH*
www.brunel.ac.uk/~icsrbicm

Abstract

This article reviews numerical algorithms for problems in solid polymer viscoelasticity in both small and large deformation. For the linear (small strain) case we review both the quasistatic and the dynamic problem and give recent results on *a posteriori* error estimation. For the large strain case we focus on the formulation and computational modelling of constrained membrane inflation, the application of which is to the thermoforming process.

Key words: Thermoforming, membranes, finite strain, viscoelasticity, adaptivity, *a posteriori* error estimates
1991 MSC: 73F15, 45D05, 65M60

1 Introduction

In this paper we describe computational models of both small strain and finite strain viscoelastic deformations of solid polymers. In the small strain case, which gives a linear model, we consider both quasistatic and dynamic

⋆ The authors would like to acknowledge the support of the US Army through its **Army Research Office** (grant # DAAD19–00–1–0421) and **European Research Office** (contract # N68171–97–M–5763), as well as the UK's **Engineering and Physical Sciences Research Council** (GR/R10844/01 and GR/M38070).

Email addresses: marianna.karamanou@brunel.ac.uk (Marianna Karamanou), simon.shaw@brunel.ac.uk (Simon Shaw), mike.warby@brunel.ac.uk (MK Warby), john.whiteman@brunel.ac.uk (JR Whiteman).

problems and, for the former, we outline recent results on *a priori* and *a posteriori* error-norm estimation. For the dynamic problem our methodology has so far been confined to goal-oriented *a posteriori* error estimation, and we outline our results for this in the context of a viscoelastic Timoshenko beam. The error estimates given can be used to drive adaptive algorithms. In these models, the viscoelasticity is modelled using a hereditary (Volterra) integral for the quasistatic problem, and internal variables for the dynamic problem.

When we move beyond small strain deformation to finite strain deformation as occurs, for example, in the large deformation of solid polymers at temperatures close to their melt point, the models become nonlinear and the theory and analysis is much less developed. One of the main practical problems here is the validity of the given proposed material model. We do not address the validity issue in this paper but instead restrict attention to a specific spring & dashpot type model, which has been used by other authors, which leads to a viscoelastic model of the differential type and which, as in the dynamic problem, can be described using internal variables. An algorithm implementing this model together with some results generated are presented.

On the topic of the algorithms used in the different parts of this paper we use the Galerkin finite element method in the space dimension throughout but the discretization in time is different in the small strain and large strain cases. For the small strain case the *a posteriori* and goal-orientated error estimation results rely on the Galerkin procedure being used in both space and time. Thus all the differential equations in this part are weakly imposed. Also, to obtain the error estimates an associated dual problem also needs to be solved and this is similarly done using Galerkin's method in both space and time. In contrast, for the finite viscoelastic model our numerical scheme involves a predictor-corrector type finite difference approach to approximately solve the nonlinear differential equations which govern how the internal variables evolve with time. This typically involves solving two elastic problems at each time step corresponding to each of the prediction and correction steps.

The presentation of the paper is as follows. In section 2 we review recent results on *a posteriori* error estimation for problems of quasistatic viscoelasticity. As we point out there, the choice of norm with respect to the time variable is crucial to achieving a computable bound which gives feedback to drive an adaptive algorithm. In section 3 we describe recent work on dynamic linear viscoelasticity problems, and we outline a generalisation of the goal-oriented error estimation approach to the wave equation as presented by Bangerth and Rannacher in [1] to viscoelasticity as modelled by internal variables. We show how this can be used in the case of a Timoshenko beam. Viscoelasticity modelled by internal variables is our link into the different context of finite deformation described in section 4. In this section we show how a spring & dashpot type model, which has been used by Le Tallec, leads to a non-

homogeneous elastic type model involving internal variables which evolve in time according to certain nonlinear ordinary differential equations. Results are presented.

2 A posteriori error estimates for linear viscostatics

In this section we review some recent results concerning *a priori* and *a posteriori* error estimation for quasistatic linear hereditary solid viscoelasticity problems. The numerical schemes use space-time Galerkin finite element methods based on discontinuous piecewise polynomials (dG) of degree $r = 0$ or 1 in time, and continuous piecewise polynomials (cG) of degree p in space. The scheme is abbreviated to dG(r)cG(p) for $r = 0, 1$. The material is drawn from [2] and [3,4] (based on the scalar case in [5]).

For a positive real number T let $\mathcal{J} := [0, T]$ denote a time interval, and for $n \in \{2, 3\}$ let Ω be a time-independent open bounded domain in $\mathbb{R}^n$ with polygonal/polyhedral boundary $\partial\Omega$. We suppose that the interior of a (linear) viscoelastic compressible body occupies Ω and is acted upon by a system of body forces $\boldsymbol{f} := (f_i(\boldsymbol{x}, t))_{i=1}^n$ for $\boldsymbol{x} := (x_i)_{i=1}^n \in \Omega$ and $t \in \mathcal{J}$, and surface tractions, $\boldsymbol{g} := (g_i(\boldsymbol{x}, t))_{i=1}^n$ for $\boldsymbol{x} \in \Gamma_N$ and $t \in \mathcal{J}$. Here $\Gamma_N := \partial\Omega \setminus \Gamma_D$ and $\Gamma_D \subseteq \partial\Omega$ is a closed (time independent) set of positive surface measure on which the body is rigidly fixed in space and time. The resulting displacement is denoted by the function $\boldsymbol{u} = (u_i)_{i=1}^n \colon \Omega \times \mathcal{J} \to \mathbb{R}^n$.

In this section we restrict ourselves to the linear theory, wherein we assume that $\boldsymbol{u}$ and $\nabla\boldsymbol{u}$ are "small" so as not to violate the assumption that Ω is time independent, and also so that the deformation can be adequately described by the "small strain" tensor, given below in (4). We assume also that $t = 0$ is a reference time such that $\boldsymbol{u} \equiv \boldsymbol{0}$ for all $t < 0$.

The results that follow arise from an application of the so-called *Johnson paradigm*, see [6], and can be regarded as an extension of the linear elasticity results given in [7]. Numerical results are not included since we are currently developing code for both the problem described below, and the dynamic problem that results when the inertia term is retained (see the following section).

In the quasistatic theory of viscoelasticity one assumes that the inertia of the body is negligible, and then Newton's second law of motion with boundary conditions gives for each $i \in \mathbb{N}(1, n) := \{1, \ldots, n\}$ that,

$$-\sigma_{ij,j} = f_i \qquad \text{in } \Omega \times \mathcal{J}, \tag{1}$$
$$u_i = 0 \qquad \text{in } \Gamma_D \times \mathcal{J}, \tag{2}$$
$$\sigma_{ij}\widehat{n}_j = g_i \qquad \text{in } \Gamma_N \times \mathcal{J}. \tag{3}$$

Here and throughout, repeated indices imply summation and $\underline{\boldsymbol{\sigma}} := (\sigma_{ij})_{i,j=1}^n$ is the symmetric stress tensor. In the linear theory the strain tensor, $\underline{\boldsymbol{\varepsilon}} := (\varepsilon_{ij})_{i,j=1}^n$, is given by,

$$\varepsilon_{ij}(\boldsymbol{u}) := \frac{1}{2}\left(\frac{\partial u_i}{\partial x_j} + \frac{\partial u_j}{\partial x_i}\right), \tag{4}$$

and with this we close this problem by introducing the following linear hereditary viscoelastic constitutive relationship between stress and strain,

$$\sigma_{ij}(\boldsymbol{u};\boldsymbol{x},t) = D_{ijkl}(\boldsymbol{x},0)\varepsilon_{kl}(\boldsymbol{u}(\boldsymbol{x},t)) - \int_0^t \frac{\partial D_{ijkl}(\boldsymbol{x},t-s)}{\partial s}\varepsilon_{kl}(\boldsymbol{u}(\boldsymbol{x},s))\,ds. \tag{5}$$

Here $\underline{\boldsymbol{D}}(\boldsymbol{x},t) := \left(D_{ijkl}(\boldsymbol{x},t)\right)_{i,j,k,l=1}^n$ is a fourth-order stress relaxation tensor satisfying the following symmetries:

$$D_{ijkl}(t) = D_{jikl}(t) = D_{ijlk}(t) \text{ but, in general, } D_{ijkl}(t) \neq D_{klij}(t). \tag{6}$$

However, we do have $D_{ijkl}(t) = D_{klij}(t)$ for $t = 0$ and $t = \infty$ in general, and for all t for isotropic materials (see e.g. [8, equations (1.10), (2.62)]). Here, and usually below, we omit the $\boldsymbol{x}$ dependence. Also, the components of $\underline{\boldsymbol{D}}$ can be assumed to be (a.e. in Ω) functions of t that are smooth enough for their first time derivatives to be of class $L_1(\mathcal{J})$. In addition, since $\underline{\boldsymbol{D}}(0)$ measures instantaneous linear elastic response we follow Hooke's law and assume positive-definiteness:

$$\gamma_{ij}\gamma_{kl}D_{ijkl}(0) > 0 \qquad \text{a.e. in } \Omega$$

for all non-zero symmetric second order tensors $\underline{\boldsymbol{\gamma}}$.

To give a weak formulation of this problem we first define the product Hilbert spaces, $\boldsymbol{H}^s(\Omega) := H^s(\Omega)^n$, for $s = 0, 1, 2, \ldots$, with inner products given by $(\boldsymbol{w},\boldsymbol{v})_s := \sum_{i=1}^n (w_i, v_i)_{H^s(\Omega)}$, for all $\boldsymbol{w}$, $\boldsymbol{v} \in \boldsymbol{H}^s(\Omega)$. These spaces have the natural norms $\|\cdot\|_s := \sqrt{(\cdot\,,\cdot)_s}$ and, of course, $\boldsymbol{L}_2(\Omega) \equiv \boldsymbol{H}^0(\Omega)$. Also, and as is usual for time dependent problems, for a Banach space $(\mathscr{B}, \|\cdot\|_{\mathscr{B}})$ we define the $L_p(0,t;\mathscr{B})$ norms by, $\|\boldsymbol{v}\|_{L_p(0,t;\mathscr{B})} := \left\| \|\boldsymbol{v}(\cdot)\|_{\mathscr{B}} \right\|_{L_p(0,t)}$. We also use the (symmetric second-order) tensor-valued L_2 space,

$$\underline{\boldsymbol{L}}_2(\Omega) := \left\{ \underline{\boldsymbol{\gamma}} = (\gamma_{ij})_{i,j=1}^n : \gamma_{ij} = \gamma_{ji} \in L_2(\Omega)\ \forall i,j \in \mathbb{N}(1,n) \right\}.$$

Using the essential boundary condition (2) we now define the (spatial) test

space,

$$H := \Big\{ \boldsymbol{v} \in \boldsymbol{H}^1(\Omega) : \boldsymbol{v} = \boldsymbol{0} \text{ on } \Gamma_D \Big\}, \tag{7}$$

and (see e.g. [2] for details) arrive at the weak problem: find $\boldsymbol{u} \in L_p(\mathcal{J}; H)$ such that,

$$A(\boldsymbol{u}(t), \boldsymbol{v}) = \langle L(t), \boldsymbol{v} \rangle + \int_0^t B(t-s; \boldsymbol{u}(s), \boldsymbol{v})\, ds \qquad \forall \boldsymbol{v} \in H, \text{ a.e. in } \mathcal{J}. \tag{8}$$

Here the bilinear forms $A : H \times H \to \mathbb{R}$ and $B : \mathcal{J} \times H \times H \to \mathbb{R}$ are defined by,

$$A(\boldsymbol{w}, \boldsymbol{v}) := \int_\Omega D_{ijkl}(0) \varepsilon_{kl}(\boldsymbol{w}) \varepsilon_{ij}(\boldsymbol{v})\, d\Omega, \tag{9}$$

$$B(t-s; \boldsymbol{w}, \boldsymbol{v}) := \int_\Omega \frac{\partial D_{ijkl}(t-s)}{\partial s} \varepsilon_{kl}(\boldsymbol{w}) \varepsilon_{ij}(\boldsymbol{v})\, d\Omega, \tag{10}$$

for all $\boldsymbol{w}$, $\boldsymbol{v} \in H$.

The symmetric bilinear form $A(\,\cdot\,,\,\cdot\,)$ is assumed to be continuous and coercive (since $\text{meas}(\Gamma_D) > 0$) on H in the respective senses:

$$|A(\boldsymbol{w}, \boldsymbol{v})| \leqslant C \|\boldsymbol{w}\|_1 \|\boldsymbol{v}\|_1 \qquad \text{and} \qquad A(\boldsymbol{v}, \boldsymbol{v}) \geqslant c \|\boldsymbol{v}\|_1^2,$$

for all $\boldsymbol{w}, \boldsymbol{v} \in H$ and where C and c are positive constants. Hence, $A(\,\cdot\,,\,\cdot\,)$ is a scalar product on H and induces the energy norm,

$$\|\boldsymbol{v}\|_H := \sqrt{A(\boldsymbol{v}, \boldsymbol{v})}$$

for all $\boldsymbol{v} \in H$. On H this norm is equivalent to the norm $\|\,\cdot\,\|_1$ and so from here on we consider $(H, a(\cdot,\cdot))$ as a Hilbert space with dual H'. The duality pairing between H and H' is denoted by $\langle\,\cdot\,,\,\cdot\,\rangle$.

We also assume that each component of $\underline{\boldsymbol{D}}$ satisfies $D_{ijkl} \in W_1^{r+1}(\mathcal{J}; L_\infty(\Omega))$, for $r = 0$ or $r = 1$. Then, the bilinear form $B(t;\,\cdot\,,\,\cdot\,)$ is continuous and similar to $A(\,\cdot\,,\,\cdot\,)$ in the sense that there exists $\phi \in L_1(\mathcal{J}; [0, \infty))$ such that

$$|B(t; \boldsymbol{w}, \boldsymbol{v})| \leqslant \phi(t) \|\boldsymbol{w}\|_H \|\boldsymbol{v}\|_H,$$

a.e. in $\mathcal{J}$ and for all $\boldsymbol{w}, \boldsymbol{v} \in H$. To motivate this assumption we need only look back to equation (10).

Below we assume that $\boldsymbol{f} \in L_p(\mathcal{J}; \boldsymbol{L}_2(\Omega))$ and $\boldsymbol{g} \in L_p(\mathcal{J}; \boldsymbol{L}_2(\Gamma_N))$, which means that,

$$\langle L(t), \boldsymbol{v} \rangle := \int_\Omega \boldsymbol{v} \cdot \boldsymbol{f}(t)\, d\Omega + \oint_{\Gamma_N} \boldsymbol{v} \cdot \boldsymbol{g}(t)\, d\Gamma \qquad \forall \boldsymbol{v} \in H. \tag{11}$$

The duality-based *a posteriori* error estimation techniques described by Eriksson et al. in [6] rely on exploiting strong (i.e. derivative) stability estimates for a continuous dual problem. By bounding derivatives of the dual solution in terms of data—which, typically, is error—we can use optimal approximation properties of the finite element space to generate *a posteriori* error estimates with optimal powers of the meshwidth and time step.

However, this approach has only limited value for (8) because the problem contains no time derivatives (there is no automatic smoothing of the temporal behaviour). For a scalar Volterra equation problem we have presented two remedies: in [9] an *a posteriori* error estimate in a weak norm; and, in [5] an *a posteriori* error estimate using the derivative of the residual. Below we outline the generalisation of these results to (8), but first we need to construct a "weak-energy" norm suited to error estimation.

We arrive at a suitable *weak-strong* norm by invoking the Riesz map $\mathscr{R}\colon H \to H'$ defined via the Riesz Representation Theorem through, $\langle \mathscr{R}\boldsymbol{w}, \boldsymbol{v}\rangle = A(\boldsymbol{w}, \boldsymbol{v})$ for all $\boldsymbol{w}, \boldsymbol{v} \in H$. Using the fact that $\mathscr{R}$ is a bijective isometry we now define a weak-strong (or a *negative-positive*) norm, for $p \in (1, \infty]$, $(a, b) \subset \mathbb{R}$ and $m \geqslant 0$, via,

$$\begin{aligned} \|\cdot\|_{W_p^{-m}(a,b;H)} &:= \|\mathscr{R}\cdot\|_{W_p^{-m}(a,b;H')} \\ &= \sup\left\{ \left| \int_a^b A(\cdot, \boldsymbol{v}(t))\, dt \right| : \begin{array}{l} \boldsymbol{v} \in \mathring{W}_q^m(a,b;H) \\ \|\boldsymbol{v}\|_{\mathring{W}_q^m(a,b;H)} = 1 \end{array} \right\}, \end{aligned} \tag{12}$$

where q is Hölder conjugate to p. The need for this norm is based on the fact that we can use it to estimate derivatives of the dual solution in terms of derivatives of data in order to measure the error in a weak temporal norm. On the other hand, this norm is only *semi-weak* since H and not H' appears on the left. Therefore, an adaptive algorithm based on estimating the error in this norm will produce strong error control in that it monitors the error in H rather than the weaker H' (see Theorem 2 below).

To construct a space-time finite element approximation of (8) we allow the test functions to be time dependent and then integrate over $\mathcal{J}$. This results in an alternative statement of the problem as: find $\boldsymbol{u} \in L_p(\mathcal{J}; H)$ such that,

$$a(\boldsymbol{u}, \boldsymbol{v}) = l(\boldsymbol{v}) \qquad \forall \boldsymbol{v} \in L_q(\mathcal{J}; H), \tag{13}$$

and,

$$a(\boldsymbol{w},\boldsymbol{v}) := \int_0^T A(\boldsymbol{w}(t),\boldsymbol{v}(t))\,dt - \int_0^T \int_0^t B(t-s;\boldsymbol{w}(s),\boldsymbol{v}(t))\,dsdt, \qquad (14)$$

$$l(\boldsymbol{v}) := \int_0^T \langle L(t),\boldsymbol{v}(t)\rangle\,dt, \qquad (15)$$

for all $\boldsymbol{w} \in L_p(\mathcal{J};H)$ and $\boldsymbol{v} \in L_q(\mathcal{J};H)$. Note that in (5), for example, we also use the symbol "l" as an integer index; a similar clash of notation will also occur below where we use k to denote time steps. Since the contexts are so different no confusion should arise.

To effect the space-time finite element discretisation of (13) we firstly discretise $\mathcal{J}$ into discrete times $0 = t_0 < t_1 < \cdots < t_N = T$, and then define the time intervals $\mathcal{J}_i := [t_{i-1}, t_i]$, and time steps, $k_i := t_i - t_{i-1} > 0$. We use $k \in L_\infty(\mathcal{J})$ to denote the piecewise constant function such that $k|_{\mathcal{J}_i} := k_i$.

During each $\mathcal{J}_i$ we construct on $\overline{\Omega}$ (in the usual way) a shape-regular triangular/tetrahedral space-mesh Ω_i, based on a set of elements $\{\Omega_{ij}\}_{j\geqslant 1}$. We use $h_i \in L_\infty(\Omega)$ to denote the piecewise constant mesh-width function used during $\mathcal{J}_i$.

During each $\mathcal{J}_i$ we define, relative to the mesh on Ω_i, the semidiscrete (spatial) finite element space,

$$H_i := \left\{ \boldsymbol{v} \in H \cap \left(C(\overline{\Omega})\right)^n : \boldsymbol{v}|_{\Omega_{ij}} \in \mathbb{P}_p(\Omega_{ij})^n \text{ for each } \Omega_{ij} \subset \Omega_i \right\}. \qquad (16)$$

For space-time finite element approximation we also define, for $r = 0$ or $r = 1$, the fully discrete finite element spaces:

$$V_r^i := \mathbb{P}_r(\mathcal{J}_i; H_i),$$
$$V_r := \left\{ \boldsymbol{v} \in L_\infty(\mathcal{J};H) : \boldsymbol{v}|_{\mathcal{J}_i} \in V_r^i \quad \forall i \in \mathbb{N}(1,N) \right\}.$$

Here $\mathbb{P}_r(\mathcal{J}_i; H_i)$ is the vector space of polynomials of degree at most r defined on $\mathcal{J}_i$ and with coefficients in H_i. Note that our approximating functions in V_r are continuous in space but, in general, temporally discontinuous at the knots $\{t_i\}_{i=1}^{N-1}$. These discontinuities allow the space-meshes to change with time and this is the basis of the dG(r)cG(p) scheme.

For $r = 0$ or 1 we form the finite element approximation to (13) as: find $\boldsymbol{U} \in V_r$ such that,

$$a(\boldsymbol{U},\boldsymbol{v}) = l(\boldsymbol{v}) \qquad \forall \boldsymbol{v} \in V_r, \qquad (17)$$

and subtracting this from (13) gives the fundamentally important Galerkin "orthogonality" relationship:

$$a(\boldsymbol{u}-\boldsymbol{U},\boldsymbol{v}) = 0 \qquad \forall \boldsymbol{v} \in V_r. \qquad (18)$$

We recall from [2] the *a priori* error estimate. (This is of course only a summary statement.)

Theorem 1 (*A priori* energy-error estimate) *If $\exists K > 0$ such that a.e. in Ω:*

- *$D_{ijkl}(t)\gamma_{ij}\gamma_{kl} \geqslant c_0 D_{ijkl}(0)\gamma_{ij}\gamma_{kl}$ for some constant $c_0 = c_0(K) > 0$, for all $t \in [0, K]$ and all $\underline{\boldsymbol{\gamma}} \in \underline{\boldsymbol{L}}_2(\Omega)$;*
- *no component $D_{ijkl}(t)$ changes sign in $[0, K]$,*

then, under standard assumptions, for dG(r)cG(1) approximation in V_r, for $r = 0, 1$, the Galerkin error, $\boldsymbol{u} - \boldsymbol{U}$, satisfies the a priori error estimate,

$$\|\boldsymbol{u} - \boldsymbol{U}\|_{L_\infty(\mathcal{J};H)} \leqslant C(T)\left(\Pi_h \left\|hD_{\boldsymbol{x}}^2\boldsymbol{u}\right\|_{L_\infty(\mathcal{J};\boldsymbol{L}_2(\Omega))} + \Pi_k \left\|k^{r+1}\partial_t^{r+1}\boldsymbol{u}\right\|_{L_\infty(\mathcal{J};H)}\right).$$

Here $C(T)$ is a discrete stability factor and Π_h, Π_k are constants. This estimate holds for $r = 1$ only if each k_i is small enough.

The structure behind the proof of the *a posteriori* error estimate as quoted below is similar to that of "Nitsche's lift", in that one first defines a continuous dual problem in order to derive an error representation formula, and then uses the stability properties of this problem and approximation-error estimates to arrive at the error bound.

The *a posteriori* error estimate that follows is based on the error representation formula,

$$l^*(\boldsymbol{e}) = a(\boldsymbol{e}, \boldsymbol{\chi}) = a(\boldsymbol{e}, \boldsymbol{\chi} - \pi\boldsymbol{\chi}) = l(\boldsymbol{\chi} - \pi\boldsymbol{\chi}) - a(\boldsymbol{U}, \boldsymbol{\chi} - \pi\boldsymbol{\chi})$$

where $\boldsymbol{\chi} \in L_q(\mathcal{J}; H)$ is the dual solution, $\boldsymbol{e} := \boldsymbol{u} - \boldsymbol{U}$ and $\pi\colon L_q(I; H) \to V_r$ is an interpolator. The term on the far right is clearly a residual.

Theorem 2 (*a posteriori* error estimate) *For any $p > 1$, any integers $0 \leqslant m, s \leqslant r + 1$, each $j \in \mathbb{N}(1, N)$, and with standard assumptions for the approximation properties of the finite element spaces, we have:*

$$\|\boldsymbol{u} - \boldsymbol{U}\|_{W_p^{-s}(0,t_j;H)} \leqslant S(t_j)\Big(t_j^s\mathcal{E}_\Omega(p, t_j; \boldsymbol{U}) + \mathcal{E}_\mathcal{J}(p, s, m, t_j; \boldsymbol{U})\Big),$$

where $S(t_j)$ is a stability factor. Here,

$$\mathcal{E}_\Omega(p, t_I; \boldsymbol{U}) := \left(\sum_{i=1}^{I}\left\|\Pi_\Omega\|h_i[\boldsymbol{f} + \nabla\cdot\underline{\boldsymbol{\sigma}}(\boldsymbol{U};\cdot)]\|_{\boldsymbol{L}_2(\Omega_i)} + \Pi_\ell\|h_i\mathscr{J}\|_{L_2(\Omega)}\right\|_{L_p(\mathcal{J}_i)}^p\right)^{\frac{1}{p}},$$

with the obvious modification for $p = \infty$, where $\|\!|\cdot|\!\|$ denotes a mesh-dependent broken norm, and $\mathscr{J}$ contains inter-element stress jumps. Also,

$$\mathcal{E}_{\mathcal{J}}(p,s,m,t_j;\boldsymbol{U}) := \urcorner_{rm}\urcorner_{rs}\Pi_1\Big(\|k^{s+m}\underline{\boldsymbol{D}}^{-\frac{1}{2}}(0)\partial_t^m\underline{\boldsymbol{\sigma}}(\boldsymbol{U};\,\cdot\,)\|_{L_p(0,t_j;\underline{\boldsymbol{L}}_2(\Omega))} + C_T\|k^{s+m}\partial_t^m\boldsymbol{g}\|_{L_p(0,t_j;\boldsymbol{L}_2(\Gamma_N))} + C_H\|k^{s+m}\partial_t^m\boldsymbol{f}\|_{L_p(0,t_j;\boldsymbol{L}_2(\Omega))}\Big).$$

In the above, Π_Ω, Π_ℓ, $\urcorner_{rm}$, $\urcorner_{rs}$, Π_1, C_H *and* C_T *are constants which are, in principle, computable.*

In this, the stability factor, $S(t)$, is associated with the continuous dual problem. We mention here only that for a viscoelastic solid we have $S(t) = O(1)$, independent of T, and refer to [10,3] for full details.

Note that because (8) contains no time derivatives we get no "free" smoothing in the temporal regularity of $\boldsymbol{u}$. The *a posteriori* error estimate allows for very rough functions by taking $m = 0$ and $s > 0$. On the other hand, when some degree of temporal regularity is present then this will be reflected in the data and we can take $s = 0$ and $m > 0$.

All of the material in this section is given in greater detail in [3,4]. In the next section we address the dynamic viscoelasticity problem.

3 A posteriori error estimates for linear viscodynamics

The quasistatic model discussed in the previous section is based on the engineering assumption that the intertia term, $\varrho\boldsymbol{u}_{tt}$, that usually appears on the left of (1) is negligible. When this assumption is not valid (e.g. in damping applications) the nature of the problem changes dramatically in that it changes from an elliptic problem to a hyperbolic problem. Information then propagates along characteristics and norm-based *a posteriori* error estimates may completely fail to resolve this form of error propagation. More generally, however, the addition of the inertia may not produce a hyperbolic problem due to the fact that engineers often use high-order dimensionally reduced models (e.g. beams, plates and shells).

For example, there is a qualitative difference between solutions of the hyperbolic) equation $u_{tt} = u_{xx}$ and the parabolic equation $u_{tt} = -u_{xxxx}$, and this difference is important in the construction of adaptive numerical schemes. The first of these is a very simple representative model of 2D/3D elasticity (modulo Huygen's principle) while the second is the Euler-Bernoulli model of a thin beam.

Consider a simple case where the initial data to the wave equation $u_{tt} = u_{xx}$ is a square pulse. Figure 1 illustrates how this initial profile is transmitted

through space-time and this is, of course, well known: it splits into two half-amplitudes with each travelling at constant speed in opposite directions. Note, in particular, that if this pulse represented an initial error then *not all of the computational domain* is polluted by this error. Hence, an effective adaptive scheme should be able to determine that in order to control errors at B and C, only the paths joining to A need significant computational effort (see Bangerth and Rannacher, [1], for more detail on this). This is a *hyperbolic* trait.

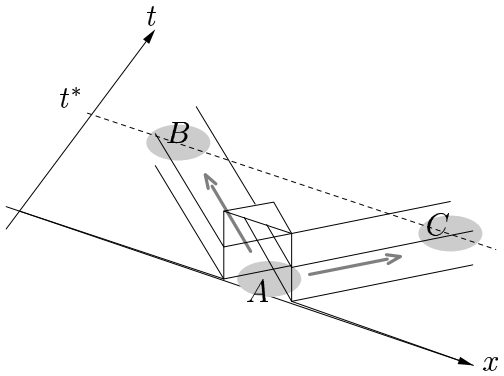

With the initial conditions $u_t(x,0) = 0$ and $u(x,0) = f(x)$, where $f(x)$ is the square pulse shown in the diagram, we obtain the famous D'Alembert solution,

$$u(x,t) = \frac{1}{2}\Big(f(x+t) + f(x-t)\Big)$$

(at least until boundary reflections occur).

Fig. 1. Example of a how initial data is propagated through the space-time domain for the standard wave equation $u_{tt} = u_{xx}$.

On the other hand, initial profiles for the beam equation $u_{tt} = -u_{xxxx}$ are split instantaneously into Fourier modes, which then propagate at frequency dependent speeds throughout the computational domain. In this case adaptive software needs to be able to control mesh-widths (in space and time) to ensure that dominant error modes are attenuated without over-compensating due to negligible modes.

To address the hyperbolic nature of dynamic viscoelasticity problems we have also begun to look at adaptivity for viscoelastic wave equations based on Bangerth and Rannacher's goal-oriented approach for the standard wave equation, see [1] (and, more generally, [11, Section 6.4] and [12]). This section summarises our results to date.

Bangerth and Rannacher in [1] propose a *goal oriented* approach which requires actually computing the dual solution. Therefore, for linear problems, the cost of implementation roughly doubles since the cost of solving the dual problem is of the same order as that for the primal problem. (In fact, for linear problems, and linear goals, the dual problem only needs to be solved once.) On the other hand a high degree of localised error control is possible, which will lead to fewer degrees of freedom in the finite element space, and hence to significant savings in computational time.

To illustrate the approach we consider an Euler-Bernoulli beam, simply supported at each end and forced only by an initial displacement. It is modelled

by the differential equation:

$$\varrho u_{tt} + (\kappa u_{xx})_{xx} - (\sigma u_x)_x = 0 \quad \text{in } Q := \Omega \times I, \tag{19}$$

where $\Omega := (0,1)$ and $I = (0,T)$. Here ϱ is the mass density per unit length and $\kappa := EI$ is the flexural rigidity. Usually, $\sigma = 0$, but we include it for the sake of performing numerical experiments comparing the beam equation, where $\sigma = 0$, to the wave equation, $\kappa = 0$. These equations are *qualitatively* different since the beam equation does not have the space-time characteristics that the wave equation has.

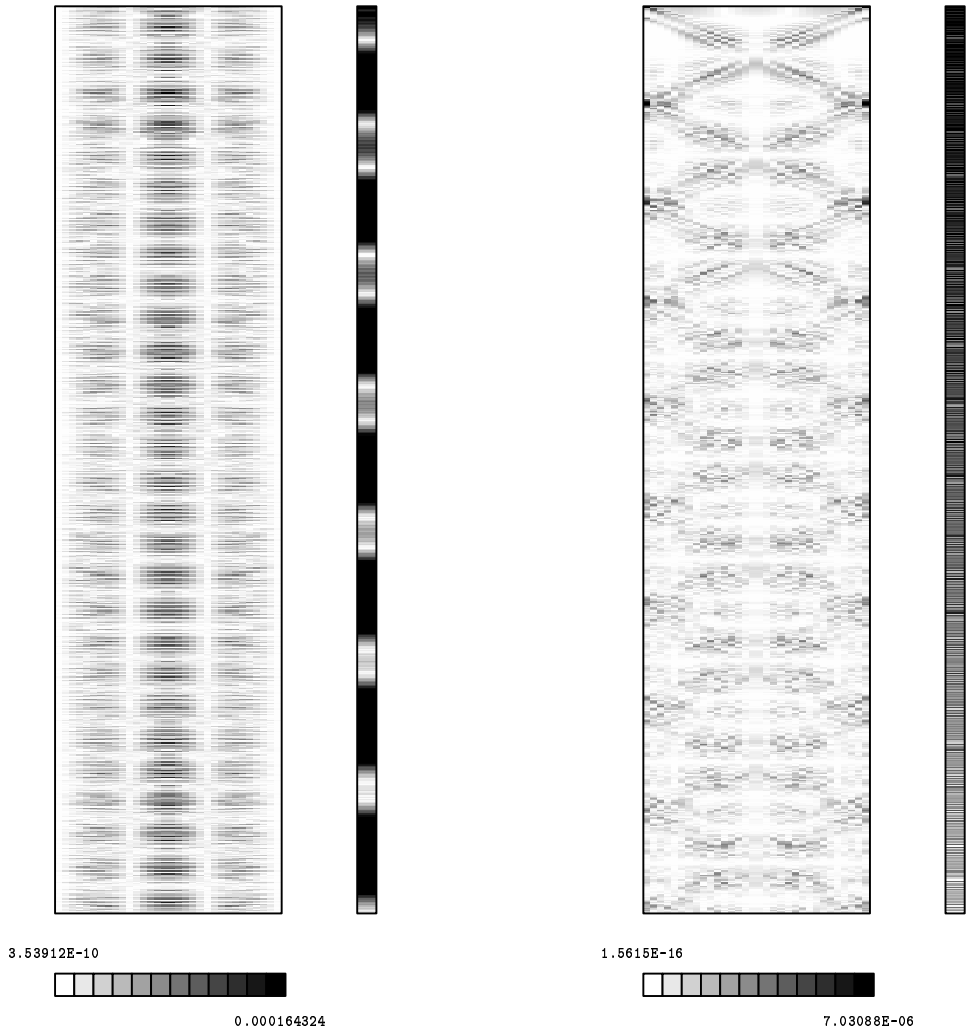

Fig. 2. Results for the beam example in equation (19). The space-time domain is $Q = (0,1) \times (0,4)$, and the parameters are $(\varrho, \kappa, \sigma) = (0.2, 1.0, 0)$, for the figure on the left, and $(\varrho, \kappa, \sigma) = (2000, 1.0, 10000)$ for the figure on the right. In these figures time increases vertically.

Using an error representation formula similar to that outlined below in Prop. 3, we apply this goal oriented method to estimating the error in the linear func-

tional (or QoI—"Quantity of Interest"),

$$\mathscr{J}(u) := \int_{t=3.95}^{t=4} \int_{x=0}^{x=1.0} u(x,t)\, dxdt.$$

In this case $\mathscr{J}(u)$ represents a localised average value, and $\mathscr{J}(e)$ corresponds to monitoring the average displacement error in a thin (in time) strip near the final time $T = 4$.

The illustration to the left in Figure 2 corresponds to the Euler-Bernoulli beam problem with $\sigma = 0$ while that on the right simulates a wave equation: $\kappa \ll \sigma, \varrho$.

The plots show how error is propagated through the space-time domain by shading, according to the horizontal scales, the space-time elements according to the absolute magnitude of their contribution to $\mathscr{J}(e)$.

We emphasise that these are *early* results and are subject to qualification. Nevertheless, they are very suggestive. Taking first the results for the simulated wave (hyperbolic) equation (on the right) we see that the error behaves exactly as expected: information travels along characteristics (as in Figure 1) and the plots of relative contributions to $\mathscr{J}(e)$ show that the error also propagates along characteristics.

The results for the (parabolic) beam problem, shown on the left, show no such structure. In these cases it is apparent that $\mathscr{J}(e)$ is composed of errors of roughly equal size throughout the space-time domain. At first it seems that there is no real application for adaptivity to this type of problem—we simply need a fine mesh *everywhere*! A closer look, however, suggests something much more subtle.

The vertical scales to the right of the large space-time plots show the evolution, with discrete time t_j, of the contributions to $\mathscr{J}(e)$. Black represents a 100% contribution while white shows 0%. We notice that for the beam problem (the figures on the left) near-white marks appear *throughout* the time stepping—and this means that at those discrete times the net contribution to the target functional $\mathscr{J}(e)$ is near-zero.

The implication is clear: it means that to control the target error we need only step to $t = T$, using a coarse mesh, until we detect the "white level" immediately prior to the functional's region of integration. At this time almost no contribution to $\mathscr{J}(e)$ has been made. Hence, we can stop the computation, refine the mesh if necessary, and use the current solution to *continue* the time stepping *without recomputing the earlier time stages*. The process could then be repeated as often as necessary and we can imagine building a space-time mesh which would remain relatively coarse away from the domain of the QoI.

It is worth noting that such a strategy could be implemented in commercial packages such as ABAQUS and ANSYS.

To add viscoelasticity we start by considering the abstract problem: find u such that,

$$\varrho\ddot{u}(t) + Au(t) = \mathscr{F}(t) - \int_0^t \varphi_t(t-s)Au(s)\,ds,$$

subject to the initial conditions $u(0) = \bar{u}$ and $\dot{u}(0) = \bar{w}$. Here A is an elliptic partial differential operator and we assume that suitable boundary conditions are also specified. For example, we could take:

- $Au = -u_{xx}$ for a viscoelastic string;
- $Au(t) = u_{xxxx}$ for the Euler Bernoulli beam;
- $Au = \nabla \cdot \sigma(u)$ for a generic 2D/3D problem,

and, indeed, many other forms modelling the Timoshenko beam, as well as various plate and shell models. It turns out that the exact form of A is not too important at this stage. We need only that the associated bilinear form is an inner product on the trial space. This bilinear form is denoted by $a(\cdot,\cdot)$ and the resulting energy norm by $\|\cdot\|_V = a(\cdot,\cdot)^{\frac{1}{2}}$, and with this we write the problem in weak form as,

$$(\varrho u(t), v)_H + a(u(t), v) = \langle \mathscr{F}, v\rangle + \int_0^t \varphi_s(t-s)a(u(s), v)\,ds,$$

where, usually, $H = L_2(\Omega)$ (or something similar) and Ω is a the spatial region within which the problem is posed. The time interval is denoted by $I = (0, T)$.

In the above, the relaxation function is given by a Prony series,

$$\varphi(t) = \varphi_0 + \sum_{j=1}^{N_\varphi} \varphi_j e^{-\alpha_j t} \qquad \text{with} \qquad \varphi_j,\ \alpha_j \geqslant 0 \qquad \text{for each } j \tag{20}$$

and with $\varphi(0) = 1$ and $\varphi_0 > 0$. With each exponential term we can associate an internal variable, ${}^\star u_j$, obeying the evolution equations,

$${}^\star\dot{u}_j(t) + \alpha_j {}^\star u(t) = \beta_j u(t) \tag{21}$$

subject to ${}^\star u_j(0) = 0$. The weak form of the momentum equation is now written as,

$$(\varrho\dot{w}(t), v)_H + a(u(t), v) - \sum_{j=1}^{N_\varphi} \gamma_j a({}^\star u_j(t), v) = \langle \mathscr{F}(t), v\rangle,$$

where $w = \dot{u}$ and $\beta_j\gamma_j = \alpha_j\varphi_j$.

We have introduced internal variables both for ease of implementation, and to match up with practitioners's work (see e.g. Johnson *et al.* in [13–16]).

At this point we break from the abstract to focus on a real engineering problem: the viscoelastic Timoshenko beam.

Let $\Omega = (0, \ell)$ denote the beam (i.e. of length ℓ) and let $I = (0, T)$ denote the time interval within which the beam's response is sought. The space-time domain is $Q = \Omega \times I$ and we seek $\boldsymbol{u} = (u_0, u_1)^T$ such that,

$$\rho A_0 \ddot{u}_0 - \frac{\partial F}{\partial x} = f_0 \qquad \text{and} \qquad \rho A_2 \ddot{u}_1 - \frac{\partial M}{\partial x} - F = f_1, \tag{22}$$

in Q, with initial data $\boldsymbol{u}(0) = \bar{\boldsymbol{u}}$ and $\dot{\boldsymbol{u}}(0) = \bar{\boldsymbol{w}}$, and given boundary conditions. In this section we also use overdots to denote partial time differentiation (because the notation gets a little crowded later on), and below we will use subscripts to denote x-differentiation. We also set $\boldsymbol{w} := \dot{\boldsymbol{u}}$.

In this model, F is the shear force and in linear viscoelasticity is given by the hereditary integral,

$$F(t) = \kappa A_0 G_0 \left(\Big(u_{0x}(t) - u_1(t)\Big) - \int_0^t \varphi_s(t-s) \Big(u_{0x}(s) - u_1(s)\Big)\, ds \right) \tag{23}$$

(note that here, and usually below, we are suppressing the x-dependence), and M is the bending moment given by,

$$M(t) = A_2 E_0 \left(u_{1x}(t) - \int_0^t \varphi_s(t-s) u_{1x}(s)\, ds \right). \tag{24}$$

(We note that the bending moment is sometimes defined with the opposite sign.) In these, φ is given by (20).

Physically, $u_0(x,t) := y(x,t)$ is the deflection of the beam's centroidal axis, and $u_1(x,t) := \theta(x,t)$ is the bending-induced slope of the cross-section. Also, ρ is the mass density of the beam; A_0 is the cross-sectional area; A_2 is the second moment of area of the cross section; κ is Timoshenko's shear correction factor (we take it as unity); G_0 is the shear modulus of the beam material; E_0 is the Young's modulus of the beam material; f_0 is the applied vertical load density per unit length; and, $f_1 = 0$ in most examples.

We assume that the first six of these quantities, as well as the φ_j and α_j, are constants.

Let the test functions be time dependent, then by integrating over the time interval, I, we can pose the problem as: find $\boldsymbol{U} := (\boldsymbol{u}, \boldsymbol{w}, \ldots {}^{\star}\boldsymbol{u}_j, \ldots)^T$ such that,

$$
\begin{aligned}
&(\boldsymbol{\varrho}\dot{\boldsymbol{w}},\boldsymbol{\psi})_Q + a(\boldsymbol{u},\boldsymbol{\psi})_Q - \sum_{j=1}^{N_\varphi} \gamma_j a({}^\star\boldsymbol{u}_j,\boldsymbol{\psi})_Q \\
&\qquad + (\boldsymbol{\varrho}\boldsymbol{u}(0),\boldsymbol{\vartheta}(0))_\Omega + (\boldsymbol{\varrho}\boldsymbol{w}(0),\boldsymbol{\psi}(0))_\Omega + \sum_{j=1}^{N_\varphi} a({}^\star\boldsymbol{u}_j(0),\boldsymbol{\eta}_j(0)) \\
&\qquad\qquad + \sum_{j=1}^{N_\varphi} a({}^\star\dot{\boldsymbol{u}}_j + \alpha_j {}^\star\boldsymbol{u}_j - \beta_j\boldsymbol{u},\boldsymbol{\eta}_j)_Q \\
&\qquad\qquad\qquad + (\boldsymbol{\varrho}\dot{\boldsymbol{u}},\boldsymbol{\vartheta})_Q - (\boldsymbol{\varrho}\boldsymbol{w},\boldsymbol{\vartheta})_Q \\
&\quad = \langle \mathscr{F},\boldsymbol{\psi}\rangle_Q + (\boldsymbol{\varrho}\bar{\boldsymbol{u}},\boldsymbol{\vartheta}(0))_\Omega + (\boldsymbol{\varrho}\bar{\boldsymbol{w}},\boldsymbol{\psi}(0))_\Omega \qquad \forall \text{ suitable } \boldsymbol{\tau}
\end{aligned} \tag{25}
$$

where p and q are conjugate Hölder indices, $\boldsymbol{\tau} = (\boldsymbol{\vartheta},\boldsymbol{\psi},\ldots\boldsymbol{\eta}_j,\ldots)^T$, and,

$$
\begin{aligned}
a(\boldsymbol{u},\boldsymbol{\psi})_Q &:= \int_0^T a(\boldsymbol{u}(t),\boldsymbol{\psi}(t))\,dt, \\
\langle \mathscr{F},\boldsymbol{\psi}\rangle_Q &:= \int_0^T \langle \mathscr{F}(t),\boldsymbol{\psi}(t)\rangle\,dt.
\end{aligned}
$$

The formulation (25) can be conveniently written as: find $\boldsymbol{U}$ such that,

$$
\mathscr{A}(\boldsymbol{U},\boldsymbol{\tau}) = \mathscr{L}(\boldsymbol{\tau}) \qquad \forall \text{ suitable } \boldsymbol{\tau}, \tag{26}
$$

where the bilinear and linear forms are defined according to the left and right sides of (25).

In this way we form a space-time finite element approximation which approximates the unknowns $\boldsymbol{U} = (\boldsymbol{u},\boldsymbol{w},\ldots,{}^\star\boldsymbol{u}_j,\ldots)$ by the finite element approximations $\boldsymbol{U}^h = (\boldsymbol{u}^h,\boldsymbol{w}^h,\ldots,{}^\star\boldsymbol{u}_j^h,\ldots)$. We are then led to consider the error $\mathscr{J}(\boldsymbol{U}-\boldsymbol{U}^h)$ in a linear functional, $\mathscr{J}$, of the solution.

This error can be represented through a duality argument, the result of which is given below. In this, $\boldsymbol{Z}$ denotes the dual solution.

Proposition 3 *We have the following error representation formula,*

$$
\mathscr{J}(\boldsymbol{U}) - \mathscr{J}(\boldsymbol{U}^h) = \mathscr{E}_0(\Delta\boldsymbol{Z}) + \mathscr{E}_1(\Delta\boldsymbol{Z}) + \mathscr{E}_2(\Delta\boldsymbol{Z}) + {}^\star\mathscr{E}(\Delta\boldsymbol{Z}), \tag{27}
$$

where $\Delta\boldsymbol{Z} = \boldsymbol{Z} - \pi\boldsymbol{Z}$, with π an interpolator to the finite element space, and,

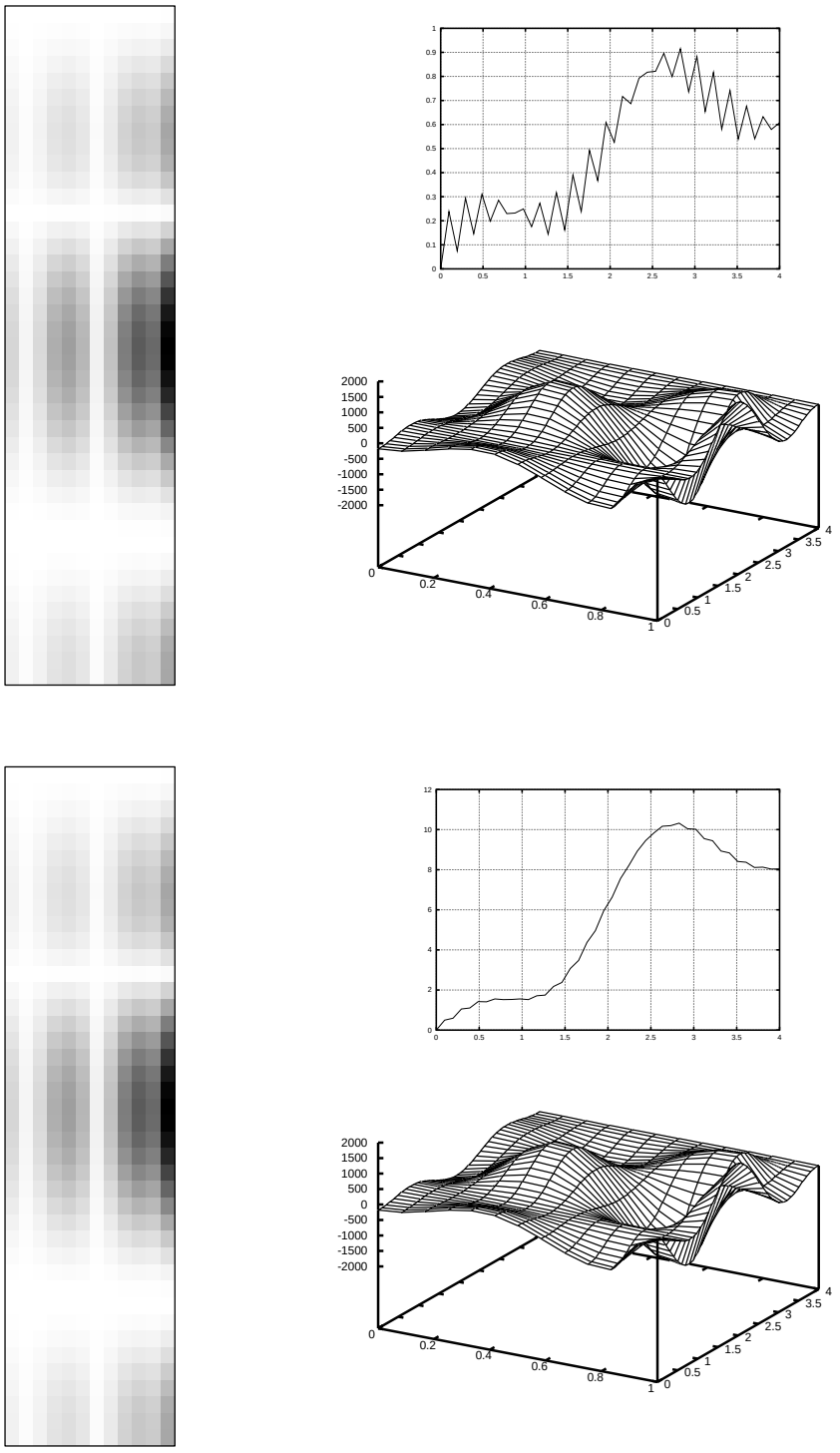

Fig. 3. Graphical realizations of the error estimators $\mathscr{J}_z(\boldsymbol{E})$, in the top figures, and $\mathscr{J}_h(\boldsymbol{E})$, in the bottom figures, with $N_e = 12$ elements and $N_t = 41$ time steps.

$$
\begin{aligned}
\mathscr{E}_0(\Delta \boldsymbol{Z}) &:= (\boldsymbol{\varrho}(\bar{\boldsymbol{u}} - \boldsymbol{u}^h(0)), \Delta\boldsymbol{\zeta}(0))_\Omega + (\boldsymbol{\varrho}(\bar{\boldsymbol{w}} - \boldsymbol{w}^h(0)), \Delta\boldsymbol{\chi}(0))_\Omega \\
&\qquad + \sum_{j=1}^{N_\varphi} a({}^\star\bar{\boldsymbol{u}}_j - {}^\star\boldsymbol{u}_j^h(0), \Delta^\star\boldsymbol{\chi}_j(0))_\Omega, \\
\mathscr{E}_1(\Delta \boldsymbol{Z}) &:= (\boldsymbol{\varrho}(\boldsymbol{w}^h - \dot{\boldsymbol{u}}^h), \Delta\boldsymbol{\zeta})_Q, \\
{}^\star\mathscr{E}(\Delta \boldsymbol{Z}) &:= \sum_{j=1}^{N_\varphi} a(\beta\boldsymbol{u}_j^h - {}^\star\dot{\boldsymbol{u}}_j^h - \alpha_j{}^\star\boldsymbol{u}_j^h, \Delta^\star\boldsymbol{\chi}_j)_Q,
\end{aligned}
$$

and,

$$
\begin{aligned}
\mathscr{E}_2(\Delta \boldsymbol{Z}) = \sum_{i=1}^{N_t} \int_{t_{i-1}}^{t_i} & (f_0 - \rho A_0 \dot{\boldsymbol{w}}_0^h + F_x^h, \Delta\chi_0)_i \\
& \qquad + (f_1 - \rho A_2 \dot{\boldsymbol{w}}_1^h + M_x^h + F^h, \Delta\chi_1)_i \, dt \\
& + \sum_{i=1}^{N_t} \int_{t_{i-1}}^{t_i} \Big((F - F^h)\Delta\chi_0 + (M - M^h)\Delta\chi_1 \Big) \Big|_{x=0}^{x=\ell} dt \\
& + \sum_{i=1}^{N_t} \int_{t_{i-1}}^{t_i} \sum_{n=1}^{N_e - 1} \Big([\![M^h]\!]_n \Delta\chi_1(x_n) + [\![F^h]\!]_n \Delta\chi_0(x_n) \Big) \, dt.
\end{aligned}
$$

where we have assumed that the space mesh is composed of N_e elements, used the broken inner product,

$$
(v, w)_i := \sum_{i=1}^{N_e} \int_{x_{i-1}}^{x_i} v(x) w(x) \, dx,
$$

and introduced the element-edge jumps,

$$
[\![v]\!]_n := \lim_{\epsilon \downarrow 0} \Big(v(x_n + \epsilon) - v(x_n - \epsilon) \Big).
$$

This result can be used in essentially two ways. We can choose a specific form for $\mathscr{J}$ and, by obtaining *a priori* stability estimates for the dual problem, and using approximation-error estimates, derive an *a posteriori* error norm estimate. On the other hand we can make an attempt to compute $\boldsymbol{Z}$ "exactly" and use the formula to indicate the error (and its space-time distribution) relative to some chosen form of $\mathscr{J}$—the "computational goal".

So far, it is the latter approach that we have concentrated on since it appears to be more effective for hyperbolic problems. Figure 3 shows a result for the Timoshenko beam equations where the problem is chosen such that the exact dual solution, required in Prop. 3, is known.

Define the error $\boldsymbol{E} := \boldsymbol{U} - \boldsymbol{U}^h$. The top half of the figure shows results for $\mathscr{J} = \mathscr{J}_z$ while the bottom half corresponds to $\mathscr{J} = \mathscr{J}_h$. The quantity

$\mathscr{J}_z(\boldsymbol{E})$ is computed by using the exact dual solution while $\mathscr{J}_h(\boldsymbol{E})$ is computed by using a computed dual solution.

The latter case is, of course, the only practical one since, in general, we have no choice but to compute the dual solution and "recover" it to a sufficiently accurate approximation. In this example $\mathscr{J}$ is a rather artificial linear functional representing a weighted average of the solution. The weight is designed such that the exact dual solution can be found.

The rectangular shaded plots on the left of Figure 3 correspond to those in Figure 2 and show the element-by-element contributions to $\mathscr{J}(\boldsymbol{E})$ according to the shading intensity. The top figures on the right show the evolution of $\mathscr{J}$ with time, while the surface plots provide another element-by-element view of $\mathscr{J}(\boldsymbol{E})$.

The dual solution was computed on the same regular space-time mesh as the primal solution (care was taken to avoid superconvergence) and, although certainly not a proof, it appears that this method can represent error propagation reasonably well while less than doubling the amount of computational effort required solve the discrete equations.

The material in this section is based on work in progress. Further details will shortly be available through the BICOM technical reports available at `www.brunel.ac.uk/~icsrbicm`.

4 A model of finite viscoelasticity

When the deformation of a body is large we get a geometrically nonlinear problem to solve and in the formulation of the problem care has to be taken to distinguish between the undeformed and deformed configurations. For a solid body it is usual to use a Lagrangian description of such a problem which involves everything being referred to a fixed reference state which we take as the undeformed configuration of the body. Each point in this state deforms according to $\boldsymbol{x} \to \boldsymbol{x} + \boldsymbol{u} =: \boldsymbol{w}$, where $\boldsymbol{u} = \boldsymbol{u}(\boldsymbol{x}, t)$ is the displacement. The usual quantities to describe the stretching and the stresses are as follows. We have the deformation gradient $\underline{\mathbf{F}} = (\partial w_i/\partial x_j)$, $\underline{\mathbf{C}} = \underline{\mathbf{F}}^T\underline{\mathbf{F}}$ and $\underline{\mathbf{B}} = \underline{\mathbf{F}}\,\underline{\mathbf{F}}^T$ are the right and left Cauchy Green deformation tensors which describe the stretching, as before $\underline{\boldsymbol{\sigma}}$ denotes the symmetric Cauchy stress tensor and $\underline{\boldsymbol{\Pi}} = (\det \underline{\mathbf{F}})\underline{\mathbf{F}}^{-1}\underline{\boldsymbol{\sigma}}$ denotes the nominal stress tensor which is not symmetric in general. In terms of $\underline{\boldsymbol{\Pi}}$ and in terms of the undeformed positions the equations

of quasistatic equilibrium when there are no body forces are given by

$$\sum_{j=1}^{3} \frac{\partial \Pi_{ji}}{\partial x_j} = 0, \quad i = 1, 2, 3, \tag{28}$$

and assuming that boundary conditions are already given, the specification of the problem becomes complete when constitutive equations connecting stress to stretch are given.

For elastic materials the stress at a given time only depends on the deformation at that time but for viscoelastic materials it depends on the entire history of the stretching as was indicated in section 2; see (5) in the case of a linear model. The constitutive relations for viscoelastic materials are usually given in the integral form (as in for example (5)) or in differential form and in some cases they can easily be expressed in either way. This is the case for the linear models given in sections 2 and 3 when the relaxation function is represented by a finite Prony series, see (20). When we have a differential form the dependence of the current stress on previous stretches is accounted for by certain quantities known as internal variables satisfying ordinary differential equations in time. Equation (21) gives the internal variable in the linear case of section 3. The simple linear models with relaxation functions given by Prony series can also be connected to various spring and dashpot configurations which are described in texts on viscoelasticity. We next describe how a particular spring dashpot representation used in the linear theory can be modified to give a model valid for the finite deformations of incompressible viscoelastic solids.

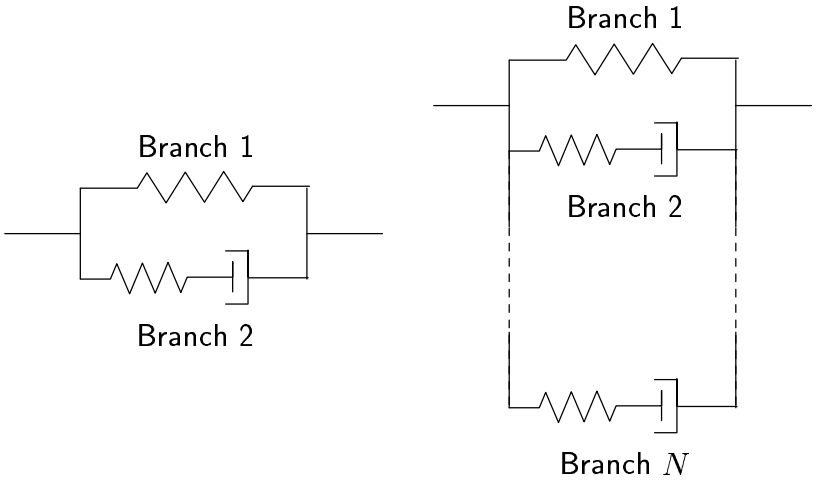

Fig. 4. Some spring–dashpot configurations

Consider the spring dashpot configurations shown in figure 4 involving parallel branches with just a spring in branch 1 and with a spring and dashpot in series in all other branches. In this set-up the stress is shared among the parallel

branches and if $\underline{\boldsymbol{\sigma}}_i$ denotes the Cauchy stress in the ith branch then

$$\underline{\boldsymbol{\sigma}} = \sum_{i=1}^{N} \underline{\boldsymbol{\sigma}}_i. \tag{29}$$

Now the deformation across each parallel branch as described by the deformation gradient $\underline{\mathbf{F}}$ is the same. Thus as branch 1 only has an elastic spring we immediately have a relation of the form

$$\underline{\boldsymbol{\sigma}}_1 = -p_1 \underline{\mathbf{I}} + \underline{\mathbf{F}} \frac{\partial W_1}{\partial \underline{\mathbf{C}}} \underline{\mathbf{F}}^T \tag{30}$$

where W_1 is the strain energy density function for this spring and where p_1 is a hydrostatic pressure term arising from the incompressibility constraint. In all other branches we have a dashpot and thus $\underline{\boldsymbol{\sigma}}_2, \cdots, \underline{\boldsymbol{\sigma}}_N$ involve a combination of a rate term (associated with the dashpot) and a non-rate term (associated with the spring) which must balance and this is what gives us an ordinary differential equation (ODE) in an internal variable which we shortly define. The precise form of the ODEs will depend on the properties of the spring and on the properties of the dashpot and in this model we assume that the springs in branches 2 to N are all new-Hookean and the dashpots are all linear viscous dashpots. The details are as follows.

In a typical branch we assume that the deformation gradient $\underline{\mathbf{F}}$ has a multiplicative decomposition

$$\underline{\mathbf{F}} = \underline{\mathbf{F}}_e \underline{\mathbf{F}}_v \tag{31}$$

with $\underline{\mathbf{F}}_e$ being the elastic part and with $\underline{\mathbf{F}}_v$ being the viscous part and we assume further that $\det \underline{\mathbf{F}}_e = \det \underline{\mathbf{F}}_v = 1$, i.e. both the elastic and viscous parts are incompressible. The stress in the neo-Hookean elastic part depends on the stretching $\underline{\mathbf{B}} = \underline{\mathbf{F}}_e \underline{\mathbf{F}}_e^T$ and the stress in the linear viscous dashpot depends on the rate of stretching $\underline{\mathbf{D}}_v$ associated with $\underline{\mathbf{F}}_v$. From the relations

$$\dot{\underline{\mathbf{F}}} = \underline{\mathbf{L}}\, \underline{\mathbf{F}}, \quad \underline{\mathbf{L}} = \left(\frac{\partial \dot{u}_i}{\partial x_j} \right), \quad \underline{\mathbf{D}} := \frac{1}{2} \left(\underline{\mathbf{L}} + \underline{\mathbf{L}}^T \right) \tag{32}$$

we obtain in the case of $\underline{\mathbf{F}}_v$ and $\underline{\mathbf{D}}_v$ the relation

$$\underline{\mathbf{D}}_v = \frac{1}{2} \left(\dot{\underline{\mathbf{F}}}_v \underline{\mathbf{F}}_v^{-1} + \underline{\mathbf{F}}_v^{-T} \dot{\underline{\mathbf{F}}}_v^T \right). \tag{33}$$

Now by introducing $\underline{\mathbf{A}} := \underline{\mathbf{F}}_v^T \underline{\mathbf{F}}_v$ as the internal variable we have that

$$\underline{\mathbf{B}}_e = \underline{\mathbf{F}}_e \underline{\mathbf{F}}_e^T = \underline{\mathbf{F}}\, \underline{\mathbf{A}}^{-1} \underline{\mathbf{F}}^T, \quad \underline{\mathbf{D}}_v = \frac{1}{2} \underline{\mathbf{F}}_v^{-T} \dot{\underline{\mathbf{A}}}\, \underline{\mathbf{F}}_v^{-1}. \tag{34}$$

As the spring and the dashpot in the branch must be in equilibrium we need to "appropriately equate" the stress arising from $\underline{\mathbf{B}}_e$ and $\underline{\mathbf{D}}_v$ which leads to the ODE in $\underline{\mathbf{A}}$. To do this we must take account of the rotation part of

the total deformation and also that with incompressible deformations only the deviatoric part of the stress is determined by the local deformation. For the rotation part let the polar decomposition of $\underline{\mathbf{F}}_e$ be given by $\underline{\mathbf{F}}_e = \underline{\mathbf{R}}_e\underline{\mathbf{U}}_e$ where $\underline{\mathbf{R}}_e$ is a proper orthogonal tensor and $\underline{\mathbf{U}}_e$ is a symmetric and positive definite. In can easily be shown that $\underline{\mathbf{B}}_e$ and $\underline{\mathbf{R}}_e\underline{\mathbf{D}}_v\underline{\mathbf{R}}_e^T$ are both objective, i.e. they transform in the appropriate way, and if the spring has constant K corresponding to a strain energy function $\frac{K}{2}(\mathrm{tr}(\underline{\mathbf{B}}_e) - 3)$ and the dashpot has viscosity η then we need to equate the deviatoric parts of

$$-p_e\underline{\mathbf{I}} + K\underline{\mathbf{B}}_e \quad \text{and} \quad -p_v\underline{\mathbf{I}} + 2\eta\underline{\mathbf{R}}_e\underline{\mathbf{D}}_v\underline{\mathbf{R}}_e^T.$$

The details are slightly messy and we get

$$\eta\underline{\mathbf{R}}_e\underline{\mathbf{F}}_v^{-T}\dot{\underline{\mathbf{A}}}\underline{\mathbf{F}}_v^{-1}\underline{\mathbf{R}}_e^T - K\underline{\mathbf{B}}_e - \frac{\gamma}{3}\underline{\mathbf{I}} = \underline{\mathbf{0}}, \quad \text{where } \gamma = 2\eta\mathrm{tr}(\underline{\mathbf{R}}_e\underline{\mathbf{D}}_v\underline{\mathbf{R}}_e^T) - K\mathrm{tr}\underline{\mathbf{B}}_e \tag{35}$$

which rearranges to

$$\eta\dot{\underline{\mathbf{A}}} - \frac{\gamma}{3}\underline{\mathbf{A}} - K(\underline{\mathbf{F}}_v^T\underline{\mathbf{R}}_e^T\underline{\mathbf{B}}_e\underline{\mathbf{R}}_e\underline{\mathbf{F}}_v) = \underline{\mathbf{0}}. \tag{36}$$

To simplify the last term note that $\underline{\mathbf{C}}_e := \underline{\mathbf{F}}_e^T\underline{\mathbf{F}}_e = \underline{\mathbf{R}}_e^T\underline{\mathbf{B}}_e\underline{\mathbf{R}}_e$. Thus

$$\underline{\mathbf{F}}_v^T\underline{\mathbf{R}}_e^T\underline{\mathbf{B}}_e\underline{\mathbf{R}}_e\underline{\mathbf{F}}_v = \underline{\mathbf{F}}_v^T\underline{\mathbf{F}}_e^T\underline{\mathbf{F}}_e\underline{\mathbf{F}}_v = \underline{\mathbf{F}}^T\underline{\mathbf{F}} = \underline{\mathbf{C}}. \tag{37}$$

For the term involving γ note that $\underline{\mathbf{D}}_v$ is associated with an incompressible deformation and hence $\mathrm{tr}(\underline{\mathbf{R}}_e\underline{\mathbf{D}}_v\underline{\mathbf{R}}_e^T) = \mathrm{tr}(\underline{\mathbf{D}}_v) = 0$ as similar tensor have the same trace. Also note that $\underline{\mathbf{B}}_e = \underline{\mathbf{F}}\underline{\mathbf{A}}^{-1}\underline{\mathbf{F}}^T$ is similar to $\underline{\mathbf{F}}^{-1}\underline{\mathbf{B}}_e\underline{\mathbf{F}} = \underline{\mathbf{A}}^{-1}\underline{\mathbf{C}}$ and thus

$$\gamma = -K\mathrm{tr}(\underline{\mathbf{A}}^{-1}\underline{\mathbf{C}}). \tag{38}$$

The ODE for $\underline{\mathbf{A}}$ can hence be written as

$$\eta\dot{\underline{\mathbf{A}}} + K\left(\frac{\mathrm{tr}(\underline{\mathbf{A}}^{-1}\underline{\mathbf{C}})}{3}\underline{\mathbf{A}} - \underline{\mathbf{C}}\right) = \underline{\mathbf{0}}, \quad \underline{\mathbf{A}}(0) = \underline{\mathbf{I}}, \tag{39}$$

and the constitutive model when $N = 2$ is

$$\underline{\boldsymbol{\sigma}} = -p\underline{\mathbf{I}} + 2\underline{\mathbf{F}}\frac{\partial W_1}{\partial\underline{\mathbf{C}}}\underline{\mathbf{F}}^T + K\underline{\mathbf{F}}\,\underline{\mathbf{A}}^{-1}\underline{\mathbf{F}}^T. \tag{40}$$

In the case when we have more branches we similarly get

$$\underline{\boldsymbol{\sigma}} = -p\underline{\mathbf{I}} + 2\underline{\mathbf{F}}\frac{\partial W_1}{\partial\underline{\mathbf{C}}}\underline{\mathbf{F}}^T + \sum_{i=2}^{N} K_i\underline{\mathbf{F}}\underline{\mathbf{A}}_i^{-1}\underline{\mathbf{F}}^T. \tag{41}$$

where $\underline{\mathbf{A}}_i$ is the internal variable for the ith branch and where K_i and η_i are the corresponding constants with $\underline{\mathbf{A}}_i$ satisfying the ODE

$$\eta_i\dot{\underline{\mathbf{A}}}_i + K_i\left(\frac{\mathrm{tr}(\underline{\mathbf{A}}_i^{-1}\underline{\mathbf{C}})}{3}\underline{\mathbf{A}}_i - \underline{\mathbf{C}}\right) = \underline{\mathbf{0}}, \quad \underline{\mathbf{A}}_i(0) = \underline{\mathbf{I}}. \tag{42}$$

In the above model if at time t_j the internal variables $\underline{\mathbf{A}}_i(t_j)$ are known at this time then the stress corresponding to the deformation $\underline{\mathbf{F}} = \underline{\mathbf{F}}(t_j)$ that is obtained is the same as the stress that is obtained with the elastic model with the strain energy density

$$W = W_1(\underline{\mathbf{F}}) + \sum_{i=2}^{N} W_i(\underline{\mathbf{F}}; \underline{\mathbf{A}}_i(t_j)), \quad W_i = \frac{K_i}{2}\left(\mathrm{tr}(\underline{\mathbf{F}}\,\underline{\mathbf{A}}_i^{-1}(t_j)\underline{\mathbf{F}}^T) - 3\right). \quad (43)$$

We make use of this here by giving at the end of this section a predictor–corrector type algorithm which involves coupling a procedure for approximately solving the ODEs for the internal variables in time with a standard procedure for solving the elastic problems in space. To simplify things slightly in what follows we will assume that $N = 2$ so that we just have one internal variable and we will just denote this by $\underline{\mathbf{A}}$.

The constitutive model described above has been used in [17] in a model of rubber tyres and because of the incompressibility assumption this required a mixed formulation in which the displacement $\boldsymbol{u}$ and the pressure p are both unknowns. We consider a simpler situation here by considering the case of modelling how a thin sheet deforms as it is forced into a mould shape by the application of a pressure. Such a deformation occurs in an industrial process known as thermoforming and when a membrane model of the thin sheet is used we avoid a mixed formulation. The details of this membrane model are briefly as follows.

We assume throughout that the undeformed body is a flat sheet of uniform thickness h_0 corresponding to the region

$$\mathcal{B} = \{x_1\boldsymbol{e}_1 + x_2\boldsymbol{e}_2 + x_3\boldsymbol{e}_3 \ : \quad (x_1, x_2) \in \Omega, \quad |x_3| < h_0/2\} \quad (44)$$

which has mid-surface $x_3 = 0$. This mid-surface deforms according to

$$(x_1, x_2, 0) \to (x_1 + u_1, x_2 + u_2, u_3) \quad (45)$$

and since material fibres normal to the mid-surface are assumed to remain normal to the sheet throughout the deformation we get a two-dimensional description of the three dimensional deformation with $\boldsymbol{u} = \boldsymbol{u}(\boldsymbol{x}) \in \mathbb{R}^3$, $\boldsymbol{x} = (x_1, x_2)^T \in \mathbb{R}^2$ as the unknown. Another of the membrane simplifications is that the stress in the direction normal to the sheet is zero. The membrane assumptions about the deformations and the stress leads to $\underline{\mathbf{C}}$ and $\underline{\boldsymbol{\sigma}}$ being of the form

$$\underline{\mathbf{C}} = \underline{\mathbf{F}}^T\underline{\mathbf{F}} = \begin{pmatrix} c_{11} & c_{12} & 0 \\ c_{12} & c_{22} & 0 \\ 0 & 0 & \lambda_3^2 \end{pmatrix}, \quad \underline{\mathbf{R}}^T\underline{\boldsymbol{\sigma}}\underline{\mathbf{R}} = \begin{pmatrix} \tilde{\sigma}_{11} & \tilde{\sigma}_{12} & 0 \\ \tilde{\sigma}_{12} & \tilde{\sigma}_{22} & 0 \\ 0 & 0 & 0 \end{pmatrix}, \quad (46)$$

where $\lambda_3^2(c_{11}c_{22} - c_{12}^2) = 1$, because of the incompressibilty, and where $\underline{\mathbf{R}}$ is the proper orthogonal tensor in the polar decomposition of $\underline{\mathbf{F}}$.

We get the weak form of equilibrium equations at time t_j in the membrane case by taking the dot product of (28) with a test vector $\boldsymbol{v}$ and integrating over the thickness. Taking account of the applied pressure $P = P(t_j)$ and using the finite element method to discretise in space gives the following problem. Find $\boldsymbol{u}^h$ from a finite element test space V^h which satisfies

$$a(\boldsymbol{u}^h, \underline{\mathbf{A}}(t_j), \boldsymbol{v}) - P(t_j) b(\boldsymbol{u}^h, \boldsymbol{v}) = 0, \quad \forall \boldsymbol{v} \in V^h \tag{47}$$

where

$$a(\boldsymbol{u}^h, \underline{\mathbf{A}}(t_j), \boldsymbol{v}) = \iint_\Omega h_0 (\underline{\boldsymbol{\Pi}}^T : \boldsymbol{\nabla} \boldsymbol{v})\, dx_1 dx_2, \tag{48}$$

$$b(\boldsymbol{u}, \boldsymbol{v}) = \iint_\Omega \boldsymbol{v} \cdot \left(\frac{\partial \boldsymbol{w}}{\partial x_1} \times \frac{\partial \boldsymbol{w}}{\partial x_2} \right) dx_1 dx_2 \tag{49}$$

$$= \frac{1}{3} \iint_\Omega \boldsymbol{v} \cdot \left(\frac{\partial \boldsymbol{w}}{\partial x_1} \times \frac{\partial \boldsymbol{w}}{\partial x_2} \right) + \boldsymbol{w} \cdot \left(\frac{\partial \boldsymbol{v}}{\partial x_1} \times \frac{\partial \boldsymbol{w}}{\partial x_2} + \frac{\partial \boldsymbol{w}}{\partial x_1} \times \frac{\partial \boldsymbol{v}}{\partial x_2} \right) dx_1 dx_2 \tag{50}$$

where $\boldsymbol{w} = (x_1, x_2, 0)^T + \boldsymbol{u}$. In this the first Piola stress $\underline{\boldsymbol{\Pi}}^T = \underline{\boldsymbol{\sigma}}\, \underline{\mathbf{F}}^{-T}$ and, as has already been indicated, the stress field that we obtain corresponds to the stress field for an elastic membrane corresponding to the strain energy function

$$W = W_1 + W_2 \quad \text{where } W_2 = \frac{K}{2} \left(\mathrm{tr}(\underline{\mathbf{A}}(t_j)^{-1} \underline{\mathbf{C}}) - 3 \right). \tag{51}$$

In our computations we take W_1 to be of the Ogden form, i.e.

$$W(\lambda_1, \lambda_2) = \sum_1^q \left(\frac{\beta_k}{\alpha_k} \right) \left(\lambda_1^{\alpha_k} + \lambda_2^{\alpha_k} + \lambda_1^{-\alpha_k} \lambda_2^{-\alpha_k} - 3 \right) \tag{52}$$

where λ_1^2 and λ_2^2 are the eigenvalues of the 2×2 principal submatrix of $\underline{\mathbf{C}}$ given in (46) and where $\alpha_1, \cdots, \alpha_q$ and $\beta_1, \cdots, \beta_q$ are constants with $\beta_k/\alpha_k > 0$. For our membrane model we have $\underline{\boldsymbol{\Pi}} = \underline{\boldsymbol{\Pi}}_1 + \underline{\boldsymbol{\Pi}}_2$ where it can be shown that

$$\underline{\boldsymbol{\Pi}}_1^T = \sum_{i=1}^2 \frac{\partial W}{\partial \lambda_i} \frac{\partial \lambda_i}{\partial \underline{\mathbf{F}}} = \frac{\partial W_1}{\partial \underline{\mathbf{F}}} \quad \text{and} \quad \underline{\boldsymbol{\Pi}}_2^T = \frac{\partial W_2}{\partial \underline{\mathbf{F}}} = K \left(\underline{\mathbf{F}}\, \underline{\mathbf{A}}^{-1} - a_{33}^{(-1)} c_{33} \underline{\mathbf{F}}^{-T} \right) \tag{53}$$

where $c_{33} = \lambda_3^2$ and where $\underline{\mathbf{A}}$ and $\underline{\mathbf{A}}^{(-1)}$ are represented in the form

$$\underline{\mathbf{A}} = \begin{pmatrix} a_{11} & a_{12} & 0 \\ a_{12} & a_{22} & 0 \\ 0 & 0 & a_{33} \end{pmatrix}, \quad \underline{\mathbf{A}}^{-1} = \begin{pmatrix} a_{11}^{(-1)} & a_{12}^{(-1)} & 0 \\ a_{12}^{(-1)} & a_{22}^{(-1)} & 0 \\ 0 & 0 & a_{33}^{(-1)} \end{pmatrix}, \quad \begin{array}{l} a_{33} = 1/(a_{11}a_{22} - a_{12}^2), \\ a_{33}^{(-1)} = 1/a_{33}. \end{array} \tag{54}$$

In these relations the partial derivatives $\partial W_i/\partial \underline{\mathbf{F}}$ and $\partial \lambda_i/\partial \underline{\mathbf{F}}$, $i = 1, 2$ are in the sense of functions of the components of the first two columns of $\underline{\mathbf{F}}$. For the computation of $\underline{\mathbf{\Pi}}_1^T$ note that by letting $\boldsymbol{v}_1$ and $\boldsymbol{v}_2$ be the normalised eigenvectors of $\underline{\mathbf{C}}$ we have

$$\lambda_i^2 = \boldsymbol{v}_i^T \underline{\mathbf{F}}^T \underline{\mathbf{F}} \boldsymbol{v}_i, \quad \boldsymbol{v}_i^T \boldsymbol{v}_i = 1$$

which when we differentiate with respect to the components of the first two columns of $\underline{\mathbf{F}}$ leads to

$$\lambda_i \frac{\partial \lambda_i}{\partial \underline{\mathbf{F}}} = (\underline{\mathbf{F}} \boldsymbol{v}_i) \boldsymbol{v}_i^T.$$

With all the stress terms being derived from W and with also $b(\boldsymbol{u}^h, \boldsymbol{v})$ in (49) being given by

$$b(\boldsymbol{u}^h, \boldsymbol{v}) = \lim_{\epsilon \to 0} \frac{g(\tilde{\boldsymbol{x}} + \boldsymbol{u}^h + \epsilon \boldsymbol{v}) - g(\tilde{\boldsymbol{x}} + \boldsymbol{u}^h)}{\epsilon}, \tag{55}$$

where $\tilde{\boldsymbol{x}} = (x_1, x_2, 0)^T$ and

$$g(\boldsymbol{w}) = \frac{1}{3} \iint_\Omega \boldsymbol{w} \cdot \left(\frac{\partial \boldsymbol{w}}{\partial x_1} \times \frac{\partial \boldsymbol{w}}{\partial x_2} \right) dx_1 dx_2 \tag{56}$$

the nonlinear system of equations that (47) generates has a symmetric Jacobian matrix.

All the above description about the stress that is obtained at time t_j corresponds to an elastic stress field requires that $\underline{\mathbf{A}}(t_j)$ is known if it is to be used and in practice we can only approximate $\underline{\mathbf{A}}(t_j)$ by using some numerical scheme to approximately solve the ODE (39). Because of the form of $\underline{\mathbf{A}}$ in (54) this is actually a system for a_{11}, a_{22} and a_{12}. We next outline our predictor–corrector type scheme for solving the finite element space problem and this ODE in time.

We use piecewise linear triangular elements in space and thus at time t the displacement field is determined by the nodal values of $\boldsymbol{u}^h(\boldsymbol{x}, t)$. As the internal variable $\underline{\mathbf{A}} = \underline{\mathbf{F}}_v^T \underline{\mathbf{F}}_v$ is a stretching type quantity and as $\underline{\mathbf{C}} = \underline{\mathbf{F}}^T \underline{\mathbf{F}}$ is constant on each triangle we assume that in the finite element discretization $\underline{\mathbf{A}}(\boldsymbol{x}, t)$ is a piecewise constant function in space. Now assuming that the state of the body is known at time t_{j-1} we do the following to obtain our approximation at time t_j.

Predict (P) step: Let $\tau = \eta/K$. We predict $\underline{\mathbf{A}}(.,t_j)$ element by element using the Euler prediction

$$\underline{\mathbf{A}}^{(0)}(\boldsymbol{x},t_j) := \underline{\mathbf{A}}(\boldsymbol{x},t_{j-1}) + \frac{\Delta t_j}{\tau}\left(\underline{\mathbf{C}}(\boldsymbol{x},t_{j-1}) - \gamma_{j-1}\underline{\mathbf{A}}(\boldsymbol{x},t_{j-1})\right),$$
$$\text{where} \quad \Delta t_j = t_j - t_{j-1}, \quad \text{and} \quad \gamma_{j-1} = \frac{1}{3}\mathrm{tr}\left(\underline{\mathbf{A}}(\boldsymbol{x},t_{j-1})^{-1}\underline{\mathbf{C}}(\boldsymbol{x},t_{j-1})\right).$$

Evaluate (E) step: We solve the anisotropic finite element elastic problem based on the latest prediction of $\underline{\mathbf{A}}(\boldsymbol{x},t_j)$ to get an approximation $\boldsymbol{u}^h(\boldsymbol{x},t_j)$.

Corrector (C) step: We attempt to improve the estimate of $\underline{\mathbf{A}}$ at time t_j using the trapezoidal rule corrector

$$\underline{\mathbf{A}}^{(1)}(\boldsymbol{x},t_j) - \underline{\mathbf{A}}(\boldsymbol{x},t_{j-1}) - \frac{\Delta t_j}{2\tau}(\underline{\mathbf{C}}(\boldsymbol{x},t_{j-1}) + \underline{\mathbf{C}}^{(1)}(\boldsymbol{x},t_j) - \gamma_{j-1}\underline{\mathbf{A}}(\boldsymbol{x},t_{j-1}) - \gamma_j^{(1)}\underline{\mathbf{A}}^{(1)}(\boldsymbol{x},t_j)) = \underline{\mathbf{0}}$$

where $\underline{\mathbf{C}}^{(1)}(\boldsymbol{x},t_j)$ is determined using the displacement obtained from the latest (E) step. In our model, in the case of a membrane, implementing this step involves solving a non-linear system of length 3 for $\underline{\mathbf{A}}^{(1)}(\boldsymbol{x},t_j)$ on each element.

Evaluate (E) step: We re-solve the anisotropic finite element elastic problem using the improved prediction of $\underline{\mathbf{A}}(\boldsymbol{x},t_j)$ from the previous corrector step to get our new approximation for $\boldsymbol{u}^h(\boldsymbol{x},t_j)$. The nodal values from the previous (E) step can be used to generate the start vector for Newtons' method to solve the nonlinear equations at this stage. With this choice of start vector the Newton iteration usually takes fewer iterations to converge than in the first (E) step.

In figure 5 we show typical results that are obtained when we use this scheme to model how a thin flat sheet, modelled as a membrane, is forced into a mould shape to which it sticks on contact and we also investigate experimentally how the final outcome depends on the material parameters. The mould used has an interior corresponding to $|x| < 1$, $|y| < 1$, $0 < z < 1$ with the mould surface corresponding to $x = \pm 1$, $y = \pm 1$, $0 < z < 1$ being rounded. The mesh shown in (a) was determined automatically by first running the model with coarser meshes to predict which parts stretch the most. In fact, with the symmetry the computations are done with the 1/8 of the region corresponding to $\{(x,y) : 0 \leqslant x \leqslant 1,\ 0 \leqslant y \leqslant x\}$. The final deformation shown in (b) was obtained by first uniformly prestretching the sheet by the factor 1.4 before the inflation started. The strain energy function W_1 used was the Jones-Treloer model corresponding to the Ogden parameters $q = 3$, $(\alpha_1,\alpha_2,\alpha_3) = (1.3, 4, -2)$, $(\beta_1,\beta_2,\beta_3) = (0.69, 0.01, -0.0122)$ in (52) and in all cases the elastic constant $K = 0.8$ with the pressure P increasing with time t according to $P = t$. The pressure is increased until all nodes are stuck to the mould. The final deformed mesh shown in (b) corresponds to $\eta = 0.5$. Using the same mesh throughout

the problem was also run with the elastic models corresponding to $\eta = 0$ and $\eta = \infty$ and with the intermediate viscoelastic values of $\eta = 0.5, 1, 2, 4, 8, 16$ and 32. In (c) we show the maximum variations between all these values of η. The maximum difference in the final displacement was only 0.11 and it was less than half of this over much of the domain indicating that this type of deformation is relatively insensitive to the elastic and viscoelastic constitutive models used.

With isotropic elastic material the principal directions of the Cauchy stress $\underline{\boldsymbol{\sigma}}$ and the deformation tensor $\underline{\mathbf{B}}$ coincide but this is no longer the case in general with the finite viscoelastic model as the eigenvectors of $\underline{\mathbf{B}} = \underline{\mathbf{F}}\,\underline{\mathbf{F}}^T$ and $\underline{\mathbf{F}}\,\underline{\mathbf{A}}^{-1}\underline{\mathbf{F}}^T$ are different. In figure 5 we indicate the size of the angle between the eigenvectors on the final deformed state. The maximum difference over all the elements is 0.66 radians (34 degrees) although on most elements it is much smaller than this. Thus, as in the case of comparing the final deformed positions, the differences are again not too large.

The results of this example are fairly typical of many such constrained inflation type deformations and seems to suggest that for many quantities of interest the results obtained are relatively insensitive to the parameters in the constitutive model. From the implementation of the scheme it is also found that it is nearly as straightforward to use the viscoelastic models as it is to just use an elastic model.

5 Conclusions

We take each section of the article in turn.

Quasistatic linear viscoelasticity. The dG(r)cG(p) scheme described in Section 2 can be considered as *expensive* because the temporally discontinuous approximation introduces two sets of unknowns at each intermediate time level. To address this we are currently working on producing similar results for a temporally continuous Galerkin approximation. This, however, is not straightforward. The test space consists of functions that are temporally piecewise constant which means, in the error representation formula, that we cannot use Galerkin orthogonality to subtract off a temporally piecewise linear interpolant. Without extra care, this leads to an *a posteriori* error estimate that is of non-optimal order in the time discretization.

Dynamic linear viscoelasticity. The goal-oriented approach used for the dynamic problem draws upon a modern development and trend in numerical analysis, and we have seen that very fine detail on the error contributions to quantities of interest can be obtained with this method. However, this approach to adaptivity requires a leap of faith: can we ever be sure that

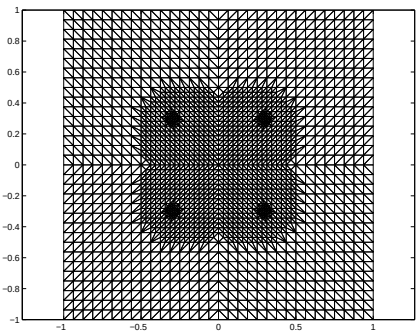

(a) Mesh

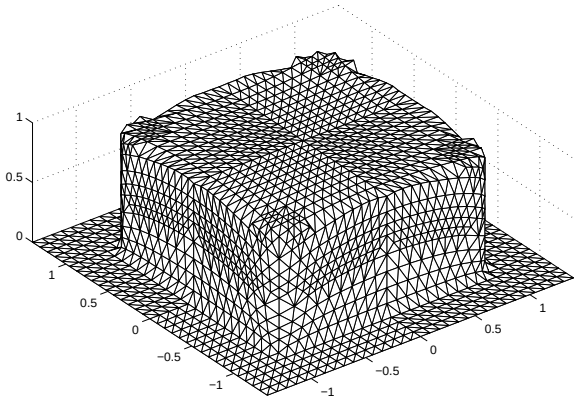

(b) Final deformation

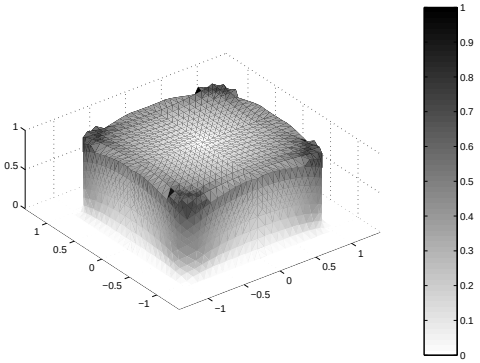

(c) Variations with $\eta = 0$, 0.5, 1, 2, 4, 8, 16, 32 and ∞. The maximum difference is 0.11. The shading indicates the fraction of this maximum over the region.

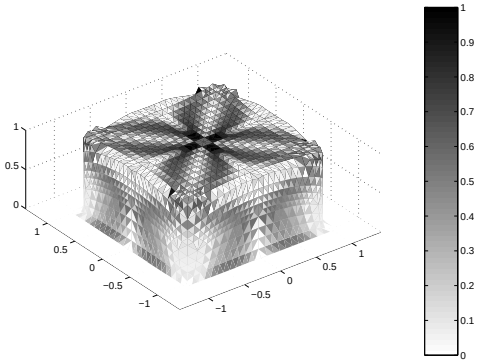

(d) Angle between principal stretch and stress directions. The maximum angle is 0.66 radians. The shading indicates the fraction of this maximum over the region.

Fig. 5. The constrained inflation of the membrane into the mould.

the dual problem is being solved with sufficient accuracy? For example, in nonlinear problems the dual problem's coefficients could be very rough and change through several orders of magnitude. What if an undetected 'locking' mechanism is at work in the discrete dual solution? This could produce completely spurious adaptivity in the primal problem.

For this reason we are also developing a more traditional norm-based *a posteriori* error estimate. In this regard we mention the related (but non-viscoelastic) results in [18, Chap. 17], for cGcG methods, and in [19–21] for dGdG methods.

Finite viscoelasticity. We have presented a finite viscoelastic model which involves solving two elastic problems at each time step corresponding to a predictor–corrector scheme to solve an ODE in time for an internal variable. This is straightforward to implement although difficulties arise if $\eta \neq 0$ with

η being small as the ODE is then "stiff" and small time steps are needed. For the type of constrained inflation deformations presented here the outcome is relatively insensitive to the material model used (elastic or viscoelastic) although when in physical situations all other modelling assumptions are very accurate (e.g. the membrane assumption and the total sticking assumption) and we need to model the process to a high accuracy then it will become more important to have the correct constitutive relations.

References

[1] W. Bangerth, R. Rannacher, Finite element approximation of the acoustic wave equation: error control and mesh adaptation, `gaia.iwr.uni-heidelberg.de/Paper/Preprint1999-15.pdf` (1999).

[2] S. Shaw, J. R. Whiteman, Numerical solution of linear quasistatic hereditary viscoelasticity problems, SIAM J. Numer. Anal 38 (1) (2000) 80—97.

[3] S. Shaw, J. R. Whiteman, *A posteriori* error estimates for space-time finite element approximation of quasistatic hereditary linear viscoelasticity problems, to appear in Comp. Meth. Appl. Mech. Engrg. See also BICOM Technical Report 03/2 at `www.brunel.ac.uk/~icsrbicm` (2003).

[4] S. Shaw, J. R. Whiteman, *A posteriori* error estimates for space-time finite element approximation of quasistatic hereditary linear viscoelasticity problems, BICOM TR03/2, `www.brunel.ac.uk/~icsrbicm` (2003).

[5] S. Shaw, J. R. Whiteman, $L_p(0,t)$ error control using the derivative of the residual for a finite element approximation of a second-kind Volterra equation, BICOM TR03/1, `www.brunel.ac.uk/~icsrbicm` (2003).

[6] K. Eriksson, D. Estep, P. Hansbo, C. Johnson, Introduction to adaptive methods for differential equations, Acta Numerica (1995) 105—158Cambridge University Press.

[7] C. Johnson, P. Hansbo, Adaptive finite element methods in computational mechanics, Comput. Methods Appl. Mech. Engrg. 101 (1992) 143—181.

[8] F. J. Lockett, Nonlinear viscoelastic solids, Academic Press, 1972.

[9] S. Shaw, J. R. Whiteman, Negative norm error control for second-kind convolution Volterra equations, Numer. Math. 85 (2000) 329–341.

[10] S. Shaw, J. R. Whiteman, Optimal long-time $L_p(0,T)$ data stability and semidiscrete error estimates for the Volterra formulation of the linear quasistatic viscoelasticity problem, Numer. Math. 88 (2001) 743—770, (BICOM Tech. Rep. 98/7 see: `www.brunel.ac.uk/~icsrbicm`).

[11] R. Rannacher, Adaptive Galerkin finite element methods for partial differential equations, `gaia.iwr.uni-heidelberg.de/Paper/Preprint1999-20.pdf` (1999).

[12] R. Rannacher, The dual-weighted-residual method for error control and mesh adaption in finite element methods, in: Whiteman [22], pp. 97—116.

[13] A. R. Johnson, Modeling viscoelastic materials using internal variables, The Shock and Vibration Digest 31 (1999) 91—100.

[14] A. R. Johnson, A. Tessler, A viscoelastic high order beam finite element, in: J. R. Whiteman (Ed.), The Mathematics of Finite Elements and Applications. MAFELAP 1996, Wiley, Chichester, 1997, pp. 333—345.

[15] A. R. Johnson, A viscoelastic hybrid shell finite element, in: Whiteman [22], pp. 87—96.

[16] A. R. Johnson, A. Tessler, M. Dambach, Dynamics of thick viscoelastic beams, Journal of Engineering Materials and Technology 119 (1997) 273—278.

[17] P. Le Tallec, C. Rahier, Numerical models of steady rolling for non-linear viscoelastic structures in finite deformations, International Journal for Numerical methods in Engineering 38 (1994) 1159—1186.

[18] K. Eriksson, D. Estep, P. Hansbo, C. Johnson, Computational differential equations, Cambridge University Press, 1996.

[19] C. Johnson, Discontinuous Galerkin finite element methods for second order hyperbolic problems, Comp. Meth. Appl. Mech. Eng. 107 (1993) 117—129.

[20] T. J. R. Hughes, G. M. Hulbert, Space-time finite element methods for elastodynamics: formulations and error estimates, Comp. Meth. Appl. Mech. Eng. 66 (1988) 339—363.

[21] G. M. Hulbert, T. J. R. Hughes, Space-time finite element methods for second-order hyperbolic equations, Comp. Meth. Appl. Mech. Eng. 84 (1990) 327—348.

[22] J. R. Whiteman (Ed.), The mathematics of finite elements and applications, X. MAFELAP 1999., Elsevier, Amsterdam, 2000.